

Random-access quantum memory using chirped pulse phase encoding

James O’Sullivan,^{1,*} Oscar W. Kennedy,^{1,*} Kamanasish Debnath,² Joseph Alexander,¹ Christoph W. Zollitsch,¹ Mantas Šimėnas,¹ Akel Hashim,^{3,4} Christopher N. Thomas,⁵ Stafford Withington,⁵ Irfan Siddiqi,^{3,4} Klaus Mølmer,² and John J. L. Morton^{1,6}

¹London Centre for Nanotechnology, UCL, 17-19 Gordon Street, London, WC1H 0AH, UK

²Department of Physics and Astronomy, Aarhus University, DK-8000 Aarhus C, Denmark

³Quantum Nanoelectronics Laboratory, Department of Physics, UC Berkeley, California 94720, USA

⁴Lawrence Berkeley National Laboratory, Berkeley, CA 94720, USA

⁵Cavendish Laboratory, University of Cambridge, JJ Thomson Ave, Cambridge CB3 0HE, UK

⁶Department of Electrical and Electronic Engineering, UCL, Malet Place, London, WC1E 7JE, UK

Quantum memories capable of faithfully storing and recalling quantum states on-demand are powerful ingredients in building quantum networks [1] and quantum information processors [2]. As in conventional computing, key attributes of such memories are high storage density and, crucially, random access, or the ability to read from or write to an arbitrarily chosen register. However, achieving such random access with quantum memories [3] in a dense, hardware-efficient manner remains a challenge, for example requiring dedicated cavities per qubit [2] or pulsed field gradients [4]. Here we introduce a protocol using chirped pulses to encode qubits within an ensemble of quantum two-level systems, offering both random access and naturally supporting dynamical decoupling to enhance the memory lifetime. We demonstrate the protocol in the microwave regime using donor spins in silicon coupled to a superconducting cavity, storing up to four multi-photon microwave pulses and retrieving them on-demand up to 2 ms later. A further advantage is the natural suppression of superradiant echo emission, which we show is critical when approaching unit cooperativity. This approach offers the potential for microwave random access quantum memories with lifetimes exceeding seconds [5, 6], while the chirped pulse phase encoding could also be applied in the optical regime to enhance quantum repeaters and networks.

Ensembles of quantum systems are natural platforms for quantum memories, given their large storage capacity. Multiple qubits can be stored by taking advantage of direct spatial addressing to access different regions of the ensemble. However, for ensembles in the solid state that offer prospects for high-density quantum memories and which typically have inhomogeneous broadening, *spectral*-addressing can be used to distinguish excitations stored collectively in the ensemble. Solid-state atomic ensembles have long coherence times for both microwave [5–9] and optical [8–10] transitions and can couple to resonant cavities facilitating read, write and control operations on the ensemble. Coherent control allows coherence times to be extended by dynamical decoupling techniques [9, 11–13] or to transfer the qubit state to a basis with longer coherence [14]. Coupling the ensemble to the cavity either in the strong coupling regime [15–19] or with cooperativity $C = 1$ facilitates writing and reading information into and out of the ensemble with unit efficiency [20, 21] ($C \equiv g^2/\kappa\Gamma$, where g is the ensemble coupling rate while κ and Γ are the half-widths of the cavity and ensemble, respectively).

One of the simplest memory protocols in inhomogeneously broadened systems is the Hahn echo [22], in which an input excitation stored within the ensemble is inverted by a single π pulse and re-emitted as an ‘echo’ at some later time. This has been used widely for retrieval of weak microwave excitations in multimode mi-

crowave [6, 23, 24] and optical [25, 26] memories and indeed formed the basis of early (classical) information storage proposals [27]. The simple Hahn echo approach is unsuitable for quantum memories, as it leads to amplified (and thus noisy) emission from the quantum systems in their excited state [28]. One solution is to use two π pulses in order to return the ensemble predominantly to the ground state before the memory is accessed [21, 29], which requires suppressing the emission of the echo that would otherwise appear after the first π pulse. A second limitation of the simple Hahn echo sequence is that it acts as a ‘first-in last-out’ memory, rather than permitting random access to stored qubits. Various approaches have been explored to address these limitations: frequency-tunable cavities can be shifted off-resonance except when the desired echo is being emitted [30]; external electric or magnetic field gradients can be used to label stored excitations and recall them in a different order [4, 31]; and AC Stark shifts can shift the emission of excitations into different time bins [32]. However, each of these methods suffers from significant experimental complexity, poor performance, or increased latency in accessing the desired memory element. In this Letter we present a simpler and more powerful approach to labelling and recalling stored qubits from an ensemble quantum memory, using chirped control pulses.

When the frequency of a control pulse is rapidly swept across the resonant frequency of an atomic transition, this can be used to perform an inversion (or π pulse) by ‘adiabatic fast passage’ (AFP) control. Such chirped pulses — with forms such as wideband, uniform rate

* These authors have contributed equally to this work

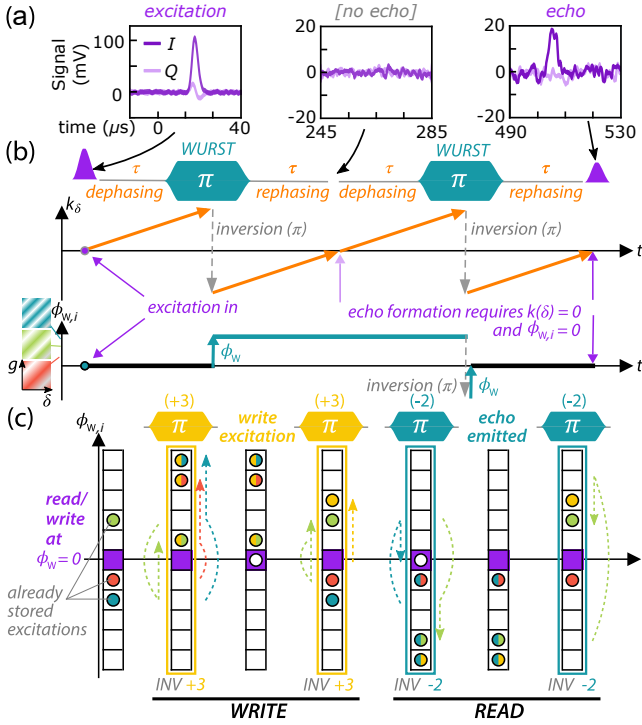


Figure 1. Using chirped pulses to silence echoes and encode quantum information. (a) A weak ($\langle n \rangle \sim 2$ photon) Gaussian microwave excitation is applied to an ensemble of Bi donor spins in silicon, followed by the application of two chirped ‘WURST’ π -pulses. A spin echo is observed only after the second WURST pulse. (b) The WURST pulse of index i inverts the phase of the ensemble and imprints a phase pattern $\phi_{W,i}$ in the space of the atom-cavity coupling g , and the frequency detuning δ . k_δ describes a wavevector of phase acquisition in frequency-space, which grows linearly in time by the precession of the inhomogeneously broadened ensemble. Excitations are stored in the ensemble at $k_\delta = \phi_W = 0$. A WURST pulse is applied at some time τ , and a further τ after the pulse the spin-wave due to inhomogeneous broadening is refocused ($k_\delta = 0$), however, the WURST-imprinted phase pattern ϕ_W remains, suppressing echo emission. A further period of τ -WURST- τ returns the excitation to $\phi_W(g, \delta) = 0$ and an echo is emitted. (c) The function $\phi_{W,i}(g, \delta)$ is defined by the chirped pulse parameters, and can be used as a storage index to encode single quantum excitations into the ensemble quantum memory. We illustrate WRITE and READ operations: By applying a particular WURST pulse (with illustrative $\phi_{W,i}$ index: +3) before and after some excitation, it becomes stored within the corresponding region in ϕ_W -space while leaving previously written excitations unaffected. The same procedure, if addressing a previously stored excitation, causes it to be emitted as an echo between the pulses.

smooth truncation (WURST) — have a number of important advantages in the context of control of ensemble quantum memories. First is their robustness to variations in the strength of the control field (e.g. laser field or microwave magnetic field) — indeed, this is a primary application of AFPs in the broader context of quantum control and is particularly attractive in the context of planar mi-

croresonators where the coupling is often highly inhomogeneous [33]. Second is that when used as a refocussing pulse to an inhomogeneously broadened ensemble, a pair of pulses must be applied in order to produce an echo. In other words, suppression of the first echo is an inherent feature of such pulses, as has been demonstrated in the optical domain [29, 34, 35], and is shown in Fig. 1(a). The third feature, which we explore in detail further below, is that the parameters of the chirped pulse (such as its amplitude and chirp rate) can be used to imprint a specific phase distribution across the atomic ensemble, allowing multiple excitations to be independently stored and retrieved within the ensemble quantum memory.

Our experiments are performed on an ensemble of bi-muth donor spins in a natural silicon host, coupled to a superconducting niobium microwave cavity at 100 mK with resonant frequency 7.093 GHz and quality factor $\sim 18,000$ (Extended Data Fig. 4 and methods). Figure 1(a) shows how two WURST π -pulses can be used to refocus an initial microwave excitation that has been absorbed by the ensemble, and confirms that *two* such pulses are required to observe an echo, as illustrated schematically in Fig. 1(b). The inhomogeneous ensemble can be decomposed into sub-ensembles each with their own spin transition frequency detuning δ and spin-cavity coupling g . Precession of the different sub-ensembles over some time τ (the ‘dephasing’ period) causes the initial excitation to evolve into a spin wave with wavevector k_δ in spin-detuning. The effect of the WURST ‘ π -pulse’ is to invert the phase acquired by the spins, and impart some additional phase shift ϕ_W , that varies across the sub-ensemble parameters δ and g , and which is a function of WURST parameters (chirp rate and pulse amplitude). Following a subsequent ‘rephasing’ period of τ , the spin wave defined by k_δ is refocused, however, due to the phase pattern defined by ϕ_W , there is no overall ensemble coherence and no collective emission of an echo. A second *identical* WURST pulse applied some time later is sufficient to unwind the phase pattern ϕ_W , so that when k_δ next returns to 0, the initial excitation is emitted as an echo. The phase patterns $\phi_{W,i}$, defined by different WURST pulses, which we refer to as the modes of the memory, provide the storage index which we exploit in our chirped-pulse quantum memory protocol, as shown in Fig. 1(c). The application of a suitably chosen WURST pulse before and after an excitation, ‘writes’ it into the ensemble without affecting previously written excitations. Applying the same pair of WURST pulses some later time is used to read out the excitation, thus enabling random access of the quantum memory. By always applying WURST pulses in identical pairs, we ensure that existing excitations already in the memory are unaffected by any read/write operation, beyond experiencing periodic inversions that assist in mitigating noise. The requirements of the WURST pulses to achieve independent storage modes are presented further below.

Before presenting the experimental demonstration of the random access protocol, we illustrate the importance

of suppressing echo emission from an inverted ensemble or during protection of the stored state (Fig. 2). Applying N_{inv} WURST π -pulses (for $N_{\text{inv}}=0-3$) before an echo sequence, as shown in Fig. 2(a), we control whether the echo is emitted from an ensemble ground state (N_{inv} even) or inverted state (N_{inv} odd), while inputting a weak excitation of $\langle n \rangle \sim 200$ microwave photons ensures that the ensemble is only weakly perturbed from the ground or inverted state when emitting. Figure 2(c) shows that echoes emitted from an inverted ensemble have larger amplitude than those emitted from a (quasi-)ground state ensemble, further supported by the dependence on the parity of N_{inv} seen in Fig. 2(d). Together, these observations indicate there has been amplification of the input signal from stimulated emission (even though the emitted echo in both cases is always weaker than the input signal due to other losses).

By increasing the delay time between the WURST pulses, we measure a coherence lifetime of this memory, $T_2 \sim 0.9$ ms (Extended Data Fig. 2). This lifetime can be extended using dynamical decoupling (DD) sequences which apply a train of repeated π -pulses [13, 36]. Using a sequence of identical WURST pulses, an echo is emitted after every two pulses (see Fig. 2). We can exploit the tunability of the WURST-induced phase shift ϕ_W to construct an alternative DD protocol in which the echo is only emitted at the end of the sequence. Introducing a second WURST pulse ('B') of different chirp rate and/or pulse amplitude to the first ('A'), we apply the sequence A[BB] $_n$ A following the initial excitation. An echo only appears after the second 'A' pulse is applied, thus suppressing unwanted emission during the DD. The resulting coherence decays are longer, and provides a measure of the memory storage lifetime, $T_2 = 2.0(2)$ ms.

Examining the echo amplitudes obtained using the A[AA] $_n$ A WURST DD sequence (in which an echo is emitted after each pair of π pulses) we find a decay time constant which is shorter than T_2 . We model this behaviour assuming a constant fraction η_{em} of the excitation in the system is lost with each echo emission, in addition to an underlying coherence decay rate equal to that seen using A[BB] $_n$ A (see methods). A fit to the data yields $\eta_{\text{em}} = 0.17(7)$ — interpreting this value as the one-way efficiency, it can be related to the cooperativity by $\eta_{\text{em}} = \frac{4C}{(1+C)^2}$ (see Ref [20]) giving $C = 0.05(2)$, in good agreement with $C = 0.07(2)$ extracted from fitting to S-parameter measurements of the cavity frequency and linewidth [37] (see methods and extended data). This one-way efficiency is larger than previously reported values for microwave quantum memories of 0.043–0.01 [6, 23, 24] due to the higher cooperativity in this sample. In a high efficiency quantum memory ($C \sim \eta_{\text{em}} \sim 1$), using DD sequences of the type introduced here will be essential to avoid the stored excitation being emitted prematurely.

Having demonstrated the ability to control echo emission using chirped pulses, we move on to an experimental demonstration of the quantum memory protocol intro-

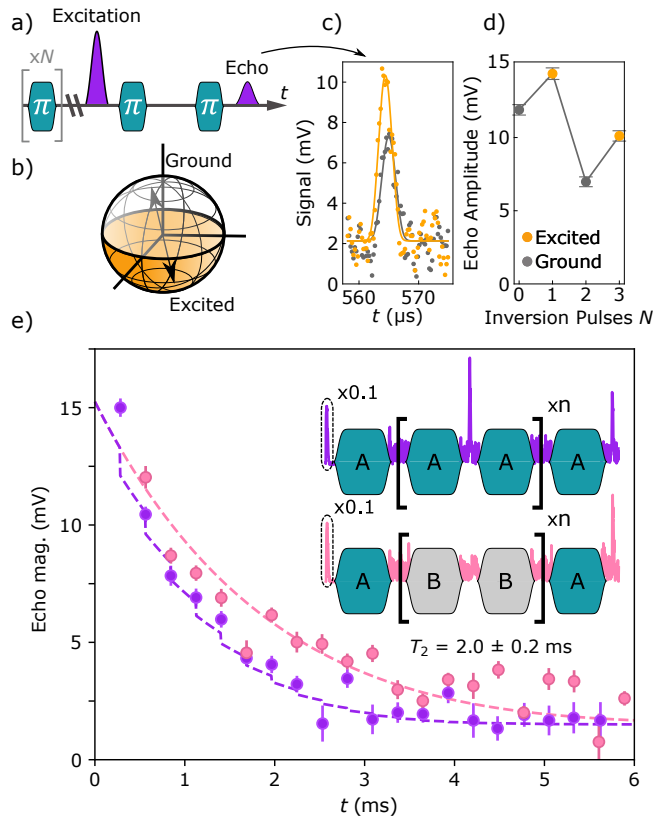


Figure 2. Demonstrating the importance of suppressed echo emission. (a) The pulse sequence used to study the echo emitted following a pair of WURST pulses as a function of the initial state of the ensemble. (b) The approximate ensemble ground and excited state in a Bloch sphere representation of the ensemble magnetisation. (c) Two example echoes emitted from the ground state ($N = 2$) or inverted state ($N = 3$). Larger amplitude echoes are seen from the inverted ensembles due to amplification of the echo, which adds noise to a quantum memory. (d) Echo amplitude as a function of N showing odd/even behaviour. The overall reduction of echo amplitude with increasing N_{inv} is likely due to gradual saturation of the spin ensemble. (e) Coherence decay rates from different WURST dynamical decoupling sequences are compared. Given identical pulses (A[AA] $_n$ A - purple) echo emission occurs after every second pulse leading to an accelerated decay in coherence compared to an (A[BB] $_n$ A - pink) pulse sequence in which only one echo is emitted, at the end. Decoherence from silenced (pink) and unsilenced (purple) T_2 measurements. A fit to the A[BB] $_n$ A data (dashed line) gives a coherence time of 2 ms, while fitting to the A[AA] $_n$ A data accounting for additional loss from repeated echoes (dashed line, see Eq. 5) gives a memory efficiency η_{em} of 0.17.

duced in Fig. 1(c). The protocol is composed of repeating blocks of the form $(\pi_j - \square - \pi_j)$ where π_j is a unique WURST π -pulse whose parameters (chirp rate and amplitude) address a particular storage index j , and \square can be i) a weak input excitation to be stored in location j of the memory; ii) an echo, constituting an excitation being retrieved from location j in memory; or iii) null,

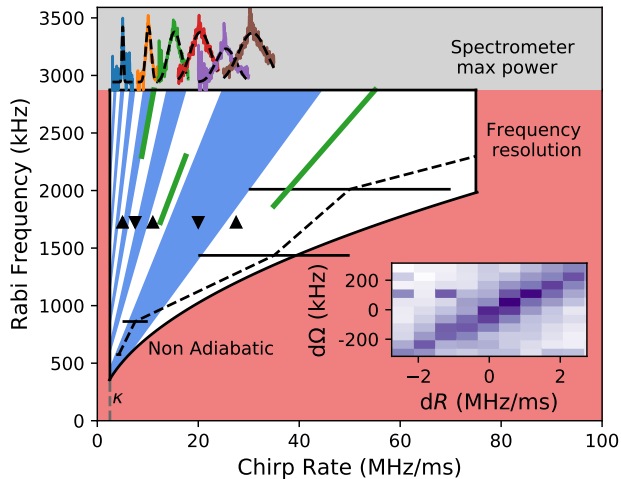


Figure 4. **Counting memory modes.** Each memory mode is determined by the phase pattern ϕ_W imparted by a WURST pulse. The parameter space where WURST pulses efficiently refocus spins is shown bounded in black. It is bounded by the cavity linewidth, the maximum spectrometer power and requirements the WURST is adiabatic. A frequency resolution limit occurs due to the homodyne scheme and would be removed in a heterodyne scheme. We measure the adiabaticity limit by thresholding echo intensity shown in the extended data and here by the black dashed line giving good agreement with the theoretical line. We measure distinctiveness of WURST pulses using AB-echo sequences. The results of sweeping the B pulse chirp rate at maximum power are inset to the top of the figure and fit by Gaussian profiles. We show a two dimensional map sweeping chirp rate and Rabi frequency in the inset. In 2D sweeps there are lines of WURST pulses which impart the same ϕ_W function to the spin ensemble. Green lines in the main panel show the line of equivalent WURST pulses from other two dimensional maps. Interpolating data from AB-echo sweeps shown here and in the extended data we determine the width of a line of equivalent WURST pulses at fixed Rabi frequency and partition the space of available WURSTs into unique WURSTs (i.e. memory modes) by constraining neighbouring WURST pulses to be separated by the half width hundredth max of this width. We show the WURST pulses used in Fig. 3 where the up/down markers refer to positive/negative chirp direction.

distinct WURST pulses at an amplitude of 0.6 V, with an equal number of WURST pulses when chirping in the reverse direction, enabling access to ~ 16 distinct storage modes in the memory.

Chirped pulse encoding can be combined with other methods such as time-bin encoding (which has been used to store up to 100 weak microwave excitations [4, 6]) in order to implement a memory offering random access to large quantum registers. We illustrate the principle using a 5-excitation register in Extended Data Fig. 6. The storage capacity of the chirped pulse encoding could be further enhanced by addressing the instrumentation-limited bounds on R and A_W , as well as by increasing

the WURST pulse duration (at the expense of slower read/write speeds and less effective DD). The memory efficiency in our experiments was primarily limited by the cooperativity ($C \sim 0.06$), and there are several practical approaches to increase this to $C \sim 1$ using Bi donors and superconducting microresonator cavities by increasing the spin-cavity coupling g and the number of resonant spins (see Ref [39]). Other factors limiting efficiency include finite coherence time and imperfect pulses. Coherence times over 300 ms have been shown for near-surface Bi donors in isotopically enriched ^{28}Si [6].

This chirped pulse protocol could also be applied to provide random read/write access in optical quantum memories. First, chirped microwave pulses such as those demonstrated here, could be applied to directly drive transitions in spin-active optical quantum memories, such as Nd in yttrium orthovanadate [32], providing dynamical decoupling and controlling access to a register of stored optical excitations. Furthermore, adiabatic fast passages (achieved using acousto-optic and electro-optic modulators) have been used to optimally invert optical transitions in demonstrations of optical quantum memories [29]. Similarly chirped optical pulses of varying parameters could allow for a random access protocol to be directly implemented in the optical domain, talking advantage of the stronger atom-cavity coupling and larger cavity bandwidth.

I. METHODS

A. Device fabrication

A float-zone silicon wafer of natural isotopic abundance is ion implanted with bismuth at a chain of energies targeting a density of 10^{17} cm^{-3} bismuth in the top $1 \mu\text{m}$ of the sample. This is annealed at 900°C for 5 minutes to incorporate the bismuth into the silicon matrix forming spin-active donors. A planar niobium microresonator is patterned on the top of the sample by liftoff. The Nb film is 100 nm thick and has a field dependent frequency (see Ref. [39]) of 7.093 GHz at a magnetic field of 46 mT.

B. Microwave measurement

The device is mounted inside a copper box which is held at 100 mK on the mixing-chamber plate of a dilution-refrigerator. Two antennae extend into the box; one short stub antenna (high insertion loss $\gtrsim 30$ dB, low coupling) is connected to a 30 dB attenuated microwave in-line and used to apply microwave excitations. Another long antenna (large coupling) is used to collect microwave signals and is connected to the amplification chain. The asymmetry results in a large collection efficiency of spin-echo signals. The signal is then routed through two circulators to a Josephson Parametric Amplifier (JPA), a quantum limited amplifier, which amplifies the signal in

reflection. The amplifier is driven via a directional coupler by a dedicated microwave source. Calibration of the JPA is given in the next section. The signal was further amplified at 4 K by a high electron mobility transistor (HEMT) and again at room temperature before being mixed down in frequency by an IQ mixer and detected using a digitiser.

Pulsed microwave signals are generated by an arbitrary waveform generator (AWG), connected to a vector source generator (VSG). These pulses are routed through either a high gain path (solid state amplifier +35 dB 3W max output) or an attenuating path (10 dB attenuation) both signal routes are actively gated using fast microwave switches. Signals are routed through the fridge before being mixed down at room temperature. A full measurement schematic is shown in Extended Data Fig. 1.

Continuous wave measurements are performed using a vector network analyser (VNA). We measured S_{21} transmission between the antennae which is modulated by the microresonator. To characterize the resonator quality factor we fit the modulation (in linear magnitude) with a Breit-Wigner-Fano function:

$$S_{21\text{Lin}}(f) = K \frac{q\kappa + f - f_0}{\kappa^2 + (f - f_0)^2} + mx + c \quad (1)$$

where K determines the size of the modulation, q is an asymmetry parameter, f_0 is the central frequency of the resonator, κ is the HWHM of the cavity and the $mx + c$ term is an approximation to the background transmission. This fits our resonance notch well and an example when the resonator is off resonance with the spins is shown in Extended Data Fig. 4.

C. System Calibration

To characterize the properties of the hybrid spin/resonator system we measure T_1 , T_2 and the Rabi frequency of the hybrid system and show these measurements in Extended Data Fig. 2. T_1 is measured by inversion recovery where the WURST pulse inverts the spin ensemble and we measure the time taken for the inverted ensemble to return to the ground state and find $T_1 \sim 14$ s. T_2 is measured using two WURST pulses to refocus a weak excitation (same strength as in Fig. 2). Varying τ allows us to measure the effect of dephasing on the echo amplitude. We fit the echo amplitude decay to a stretched exponential returning a coherence time of ~ 900 μ s and a stretch factor of 2.8 ± 0.7 , consistent with typical values found in natural silicon of ~ 2.3 [40, 41].

To measure the Rabi frequency, Ω , we apply a θ rotation pulse followed 10 ms later by a detection sequence with VSG output power of -20 dBm sent through the high gain path. The θ -pulse is chosen to match the duration and shape of the excitations used in the memory sequence in Fig. 3. The heavily damped envelope to sinusoidal Rabi oscillations (shown in extended data) is due to a large inhomogeneity in single spin coupling, g_0 ,

across the ensemble. We fit a decaying cosine function to the echo amplitude, allowing us to extract an approximate π pulse amplitude of 0.435 (where 1 is the maximum pulse amplitude at the chosen VSG output power) giving $\Omega = 125$ kHz.

Using T_1 and Ω we calibrate the photon number in the resonator. The Purcell effect limits $1/T_1 = g_0^2/\kappa$, allowing a measure of average spin-resonator coupling g_0 . The different κ dependence from Ref. [42] is due to the definition of κ being the HWHM in this work and FWHM in Ref. [42]. At the centre of the line $\kappa \sim 200$ kHz, $T_1 = 14.7$ s giving $g_0 \sim 120$ Hz (g_0 varies across the ensemble and this number is indicative). The Rabi frequency can be written as $\Omega = 2g_0\sqrt{n}$ which allows us to calibrate the photon number $n \sim 2.7 \times 10^5$ for the π pulse above. We can rescale this to the photon number to the memory sequence in Fig. 3 and find $\langle n \rangle \sim 600$ photons for the memory protocol.

The use of a JPA in measurements was essential to perform experiments at low photon numbers. Such amplifiers are prone to saturation and nonlinearity with large input signals. We calibrate the JPA to determine the onset and extent of the nonlinear regime, and any additional distortions that may be present. For comparison, the same measurements were repeated with the JPA turned off, using only a HEMT at 4 K for amplification. We confirm that for Fig. 3 the echo signals are well into the linear regime but the input excitations are in the nonlinear regime of the JPA and are prone to distortion. The HEMT remains linear and un-distorted at all powers, as expected. JPA calibrations are shown in Extended Data Fig. 3.

D. Cooperativity

Cooperativity in a hybrid micro-resonator spin system can be measured by the dispersive shift to the resonator frequency (f), and the increased half-width half max of the resonator frequency response (κ) [43]:

$$f = f_0 - \frac{g_{\text{ens}}^2 \Delta}{\Delta^2 + \gamma^2} \quad (2)$$

$$\kappa = \kappa_0 + \frac{g_{\text{ens}}^2 \gamma}{\Delta^2 + \gamma^2} \quad (3)$$

where κ_0 and f_0 are respectively the half width and frequency of the resonator in the absence of spins, and the detuning $\Delta = (B_0 - B_R) \times \partial f / \partial B_0$, where B_R is the magnetic field at which spins and resonator are resonant. Fitting equations 2 and 3 to our data gives $C \sim 0.067$ as shown in Extended Data Fig. 4.

We also extract the cooperativity from T_2 measurements with CPMG sequences in Fig. 2 by modelling the echo intensity as a function of echo number and considering the reduction of energy in the echo field with repeated

emission. In A[BB] $_n$ A sequences the echo is emitted after the final A pulse. As (i) WURST pulses efficiently refocus spins and (ii) only one echo forms, we attribute any change in echo intensity to dephasing of the spins. We fit the echo intensity $A_{\text{sil}}(t)$ to extract the dephasing time T_2 using

$$A_{\text{sil}}(t) = \sqrt{A_0^2 \exp(-2t/T_2) + K^2}, \quad (4)$$

where A_0 is the echo amplitude at time $t = 0$, T_2 is the dephasing time and K is the background giving a dephasing time of $T_2 = 2.0 \pm 0.2$ ms for a refocusing rate of 7.1 kHz. We model the echo amplitude in A[AA] $_n$ A sequences by assuming that every time an echo forms, a constant fraction of the energy stored in the echo field is lost and that in between echo emission the echo field dephases as in A[BB] $_n$ A sequences. We model the echo amplitude by

$$A(t) = \sqrt{A_0^2 \exp(-2t/T_2) \times (1 - \eta_{\text{em}})^N + K^2} \quad (5)$$

where η_{em} is the efficiency with which energy is emitted from the echo field to the cavity, N is the number of echoes which have occurred before time t . This is fit with one free parameter, η_{em} and is shown in Fig. 2.

Using Equation 17 from Ref. [20] we relate the one-way efficiency to the cooperativity by

$$\eta_{\text{em}} = \frac{4C}{(1+C)^2} \quad (6)$$

giving $C = 0.047$ in close agreement to the value extracted in the more typical method by measuring effects on the resonator.

E. WURST Pulses

1. Input Output Theory

Wideband uniform rate smooth truncation (WURST) pulses can be characterized by frequency and amplitude modulation (FM and AM respectively)

$$f_{\text{W}}(t) = -\frac{\Gamma_{\text{W}}}{2} + \frac{\Gamma_{\text{W}}}{T_{\text{W}}}t, \quad (7)$$

$$A_{\text{W}}(t) = 1 - \left| \sin\left(\pi \frac{t - T_{\text{W}}/2}{T_{\text{W}}}\right) \right|^N,$$

where Γ_{W} is the bandwidth of the WURST pulse, T_{W} is the WURST pulse duration and N is the WURST pulse index, in this work we use $N = 20$ pulses.

The FM results in a time varying phase of the output pulse

$$\phi(t) = \int_0^t f_{\text{W}}(t') dt' + \phi_0, \quad (8)$$

where ϕ_0 is the phase of the WURST pulse. The I and Q pulse quadratures applied by the AWG are

$$I(t) = A_{\text{W}}(t) \sin \phi(t),$$

$$Q(t) = A_{\text{W}}(t) \cos \phi(t), \quad (9)$$

The WURST pulse is modulated by the cavity described by input/output theory [44, 45] where

$$\dot{X}(t) = \sqrt{\kappa_C} I(t) - \frac{\kappa}{2} X(t),$$

$$\dot{Y}(t) = \sqrt{\kappa_C} Q(t) - \frac{\kappa}{2} Y(t), \quad (10)$$

where κ_C is the coupling linewidth of the cavity and κ is the loaded linewidth of the cavity. Increasing the bandwidth of the WURST pulse above the bandwidth of the cavity shortens the effective WURST pulse duration.

2. Limits on WURST Pulses

In Fig. 4, a region of suitable WURST pulses — WURST pulses which invert a large fraction of the spin ensemble — is mapped out based on both theory and experiment described in this section. Using pulse sequences such as that in Fig. 1(a) (excitation followed by two identical WURST pulses) we have measured the refocusing efficiency. We measure the amplitude of the first (nominally silenced) and second echo and present them as a function of the WURST pulse bandwidth and amplitude in Extended Data Fig. 8. A ‘good’ WURST pulse results in no echo after the first WURST, and a loud echo after the second.

By thresholding the lines we determine regions where WURST pulses adiabatically refocus a large fraction of spins. The constraint that the second echo must have a suitable magnitude (85 mV) gives the experimental boundary to suitable WURST pulses shown in Fig. 4 based on adiabaticity.

This is supported by a theoretical treatment [38].

$$Q_{\text{min}} = 2\pi\nu^2/R \gg 1, \quad (11)$$

where Q_{min} is an adiabaticity factor R is the chirp rate, ν is the nutation frequency (how quickly the spin precesses around the effective field), and R is the chirp rate. ν is minimal (and equal to the Rabi frequency) when the WURST frequency is the same as the spin frequency. We choose a minimum g_0 for spins to be refocused and solve this equation for $Q_{\text{min}} = 1$ finding a lower limit on pulse strength.

In the homodyne scheme used in this work there is a limit placed by the finite frequency resolution we can imprint onto WURST pulses. The effective duration of the WURST pulse, $T_{\text{W,eff}} = 2\kappa T_{\text{W}}/\Gamma_{\text{W}}$, is the time the WURST pulse of duration T_{W} and total bandwidth Γ_{W} takes to chirp across the cavity frequency 2κ . The inverse of this time gives an indication of the minimum frequency that can be resolved by modulating the pulse.

This frequency must be less than the cavity bandwidth placing a limit on the maximum Γ_W which can be used,

$$\Gamma_W \ll \kappa^2 T_W = 37 \text{ MHz}, \quad (12)$$

The maximum spectrometer power limits the power of WURSTs we can apply and is shown as the top boundary in Fig. 4. This line cannot be increased to arbitrarily high powers using higher power amplifiers as the superconducting resonators will limit the maximum power. There is also a minimum WURST bandwidth imposed by the cavity bandwidth.

3. WURST pulse distinctiveness

We partition the space of suitable WURSTs into ‘distinct’ WURST pulses to estimate the memory capacity. We partition this region based upon two-WURST echo sequences where the first and second WURST pulse have different properties. Inset to Fig. 4 is the echo amplitude as the amplitude and chirp rate of the B pulse is varied. This sequence results in strong echoes along a line in with positive gradient. In the main text we explain that this line of equivalent pulses is due to the acquisition of a dynamic phase. Together with other two dimensional and one dimensional maps varying a B-pulse parameter we interpolate the gradient and width of the line of equivalent pulses across the space of WURST pulses giving good inversion and use this interpolation to count WURST pulses. This interpolation is shown in Extended Data Fig. 9 with the results in Fig. 4.

II. ACKNOWLEDGEMENTS

We thank Philippe Goldner for insightful discussions relating to the implementation of this protocol in the optical domain. We thank the UK National Ion Beam Centre (UKNIBC) where the silicon samples were ion implanted and Nianhua Peng who performed the ion implantation. This work has received funding from the U.K. Engineering and Physical Sciences Research Council (EPSRC), through UCLQ postdoctoral fellowships (O.W.K, M.S.) Grant No. EP/P510270/1 and a Doctoral Training Grant (J.O’S.). J.J.L.M. acknowledges funding from the European Research Council under the European Union’s Horizon 2020 research and innovation programme (Grant agreement No. 771493 (LOQO-MOTIONS)).

III. AUTHOR CONTRIBUTIONS

J.O’S and O.W.K. performed the experiments with assistance from C.W.Z.. J.O’S, O.W.K. and J.J.L.M. analysed the data with input from J.A. and M.S.. J.A. designed the random access protocol with input from O.W.K., J.O’S and J.J.L.M.. K.D. and K.M. performed numerical analyses and the analytical treatment. C.T. and S.W. fabricated the device. A.H. and I.S. assembled, tested, and provided scientific support in the operation of the JPA. J.O’S, O.W.K. and J.J.L.M. wrote the manuscript with input from all authors.

-
- [1] H Jeff Kimble. The quantum internet. *Nature*, 453(7198):1023–1030, 2008.
 - [2] Matteo Mariantoni, Haiyan Wang, Takashi Yamamoto, Matthew Neeley, Radoslaw C Bialczak, Yu Chen, Mike Lenander, Erik Lucero, Aaron D O’Connell, Daniel Sank, et al. Implementing the quantum von neumann architecture with superconducting circuits. *Science*, 334(6052):61–65, 2011.
 - [3] N Jiang, Y-F Pu, W Chang, C Li, S Zhang, and L-M Duan. Experimental realization of 105-qubit random access quantum memory. *npj Quantum Information*, 5(1):1–6, 2019.
 - [4] Hua Wu, Richard E George, Janus H Wesenberg, Klaus Mølmer, David I Schuster, Robert J Schoelkopf, Kohei M Itoh, Arzhang Ardavan, John JL Morton, and G Andrew D Briggs. Storage of multiple coherent microwave excitations in an electron spin ensemble. *Physical Review Letters*, 105(14):140503, 2010.
 - [5] Gary Wolfowicz, Alexei M Tyryshkin, Richard E George, Helge Riemann, Nikolai V Abrosimov, Peter Becker, Hans-Joachim Pohl, Mike LW Thewalt, Stephen A Lyon, and John JL Morton. Atomic clock transitions in silicon-based spin qubits. *Nature Nanotechnology*, 8(8):561–564, 2013.
 - [6] V Ranjan, J O’Sullivan, E Albertinale, B Albanese, T Chanelière, T Schenkel, D Vion, D Esteve, E Flurin, JJJ Morton, and P Bertet. Multimode storage of quantum microwave fields in electron spins over 100 ms. *arXiv preprint arXiv:2005.09275*, 2020.
 - [7] M Steger, K Saeedi, MLW Thewalt, JJJ Morton, H Riemann, NV Abrosimov, P Becker, and H-J Pohl. Quantum information storage for over 180 s using donor spins in a 28si “semiconductor vacuum”. *Science*, 336(6086):1280–1283, 2012.
 - [8] Antonio Ortu, Alexey Tiranov, Sacha Welinski, Florian Fröwis, Nicolas Gisin, Alban Ferrier, Philippe Goldner, and Mikael Afzelius. Simultaneous coherence enhancement of optical and microwave transitions in solid-state electronic spins. *Nature Materials*, 17(8):671–675, 2018.
 - [9] Nir Bar-Gill, Linh M Pham, Andrejs Jarmola, Dmitry Budker, and Ronald L Walsworth. Solid-state electronic spin coherence time approaching one second. *Nature Communications*, 4(1):1–6, 2013.
 - [10] Denis D Sukachev, Alp Sipahigil, Christian T Nguyen, Mihir K Bhaskar, Ruffin E Evans, Fedor Jelezko, and Mikhail D Lukin. Silicon-vacancy spin qubit in diamond: a quantum memory exceeding 10 ms with single-shot state readout. *Physical Review Letters*, 119(22):223602, 2017.

- [11] Boris Naydenov, Florian Dolde, Liam T Hall, Chang Shin, Helmut Fedder, Lloyd CL Hollenberg, Fedor Jelezko, and Jörg Wrachtrup. Dynamical decoupling of a single-electron spin at room temperature. *Physical Review B*, 83(8):081201, 2011.
- [12] Herman Y Carr and Edward M Purcell. Effects of diffusion on free precession in nuclear magnetic resonance experiments. *Physical Review*, 94(3):630, 1954.
- [13] Saul Meiboom and David Gill. Modified spin-echo method for measuring nuclear relaxation times. *Review of Scientific Instruments*, 29(8):688–691, 1958.
- [14] John JL Morton, Alexei M Tyryshkin, Richard M Brown, Shyam Shankar, Brendon W Lovett, Arzhang Ardavan, Thomas Schenkel, Eugene E Haller, Joel W Ager, and SA Lyon. Solid-state quantum memory using the 31 p nuclear spin. *Nature*, 455(7216):1085–1088, 2008.
- [15] Y Kubo, FR Ong, Patrice Bertet, Denis Vion, V Jacques, D Zheng, A Dréau, J-F Roch, Alexia Auffèves, Fedor Jelezko, et al. Strong coupling of a spin ensemble to a superconducting resonator. *Physical Review Letters*, 105(14):140502, 2010.
- [16] Stefan Weichselbaumer, Matthias Zens, Christoph W Zollitsch, Martin S Brandt, Stefan Rotter, Rudolf Gross, and Hans Huebl. Echo trains in pulsed electron spin resonance of a strongly coupled spin ensemble. *Physical Review Letters*, 125(13):137701, 2020.
- [17] S Probst, H Rotzinger, S Wünsch, P Jung, M Jerger, M Siegel, AV Ustinov, and PA Bushev. Anisotropic rare-earth spin ensemble strongly coupled to a superconducting resonator. *Physical Review Letters*, 110(15):157001, 2013.
- [18] DI Schuster, AP Sears, E Ginossar, L DiCarlo, L Frunzio, JLL Morton, H Wu, GAD Briggs, BB Buckley, DD Awschalom, et al. High-cooperativity coupling of electron-spin ensembles to superconducting cavities. *Physical Review Letters*, 105(14):140501, 2010.
- [19] Tian Zhong, Jonathan M Kindem, Jake Rochman, and Andrei Faraon. Interfacing broadband photonic qubits to on-chip cavity-protected rare-earth ensembles. *Nature communications*, 8(1):1–7, 2017.
- [20] Mikael Afzelius, N Sangouard, Göran Johansson, MU Staudt, and CM Wilson. Proposal for a coherent quantum memory for propagating microwave photons. *New Journal of Physics*, 15(6):065008, 2013.
- [21] Brian Julsgaard, Cécile Grezes, Patrice Bertet, and Klaus Mølmer. Quantum memory for microwave photons in an inhomogeneously broadened spin ensemble. *Physical Review Letters*, 110(25):250503, 2013.
- [22] Erwin L Hahn. Spin echoes. *Physical Review*, 80(4):580, 1950.
- [23] S Probst, H Rotzinger, AV Ustinov, and PA Bushev. Microwave multimode memory with an erbium spin ensemble. *Physical Review B*, 92(1):014421, 2015.
- [24] C Grezes, Brian Julsgaard, Y Kubo, M Stern, T Umeda, J Isoya, H Sumiya, H Abe, S Onoda, T Ohshima, et al. Multimode storage and retrieval of microwave fields in a spin ensemble. *Physical Review X*, 4(2):021049, 2014.
- [25] Marko Lovrić, Dieter Suter, Alban Ferrier, and Philippe Goldner. Faithful solid state optical memory with dynamically decoupled spin wave storage. *Physical Review Letters*, 111(2):020503, 2013.
- [26] Alexander I Lvovsky, Barry C Sanders, and Wolfgang Tittel. Optical quantum memory. *Nature Photonics*, 3(12):706–714, 2009.
- [27] AG Anderson, RL Garwin, EL Hahn, JW Horton, GL Tucker, and RM Walker. Spin echo serial storage memory. *Journal of Applied Physics*, 26(11):1324–1338, 1955.
- [28] Jérôme Ruggiero, Jean-Louis Le Gouët, Christoph Simon, and Thierry Chanelière. Why the two-pulse photon echo is not a good quantum memory protocol. *Physical Review A*, 79(5):053851, 2009.
- [29] Vianney Damon, Matthieu Bonarota, Anne Louchet-Chauvet, Thierry Chanelière, and Jean-Louis Le Gouët. Revival of silenced echo and quantum memory for light. *New Journal of Physics*, 13(9):093031, 2011.
- [30] Yuimaru Kubo, Cecile Grezes, Andreas Dewes, T Umeda, Junichi Isoya, H Sumiya, N Morishita, H Abe, S Onoda, T Ohshima, et al. Hybrid quantum circuit with a superconducting qubit coupled to a spin ensemble. *Physical Review Letters*, 107(22):220501, 2011.
- [31] Barbara Kraus, Wolfgang Tittel, Nicolas Gisin, Mattias Nilsson, Stefan Kröll, and J Ignacio Cirac. Quantum memory for nonstationary light fields based on controlled reversible inhomogeneous broadening. *Physical Review A*, 73(2):020302, 2006.
- [32] Tian Zhong, Jonathan M Kindem, John G Bartholomew, Jake Rochman, Ioana Craiciu, Evan Miyazono, Marco Bettinelli, Enrico Cavalli, Varun Verma, Sae Woo Nam, et al. Nanophotonic rare-earth quantum memory with optically controlled retrieval. *Science*, 357(6358):1392–1395, 2017.
- [33] Anthony J Sigillito, Hans Malissa, Alexei M Tyryshkin, Helge Riemann, Nikolai V Abrosimov, Peter Becker, H-J Pohl, Mike LW Thewalt, Kohei M Itoh, John JL Morton, et al. Fast, low-power manipulation of spin ensembles in superconducting microresonators. *Applied Physics Letters*, 104(22):222407, 2014.
- [34] KI Gerasimov, MM Minnegaliev, SA Moiseev, RV Urmancheev, T Chanelière, and A Louchet-Chauvet. Quantum memory in an orthogonal geometry of silenced echo retrieval. *Optics and Spectroscopy*, 123(2):211–216, 2017.
- [35] Matthieu Bonarota, Julian Dajczgewand, Anne Louchet-Chauvet, Jean-Louis Le Gouët, and Thierry Chanelière. Photon echo with a few photons in two-level atoms. *Laser Physics*, 24(9):094003, 2014.
- [36] Lorenza Viola, Emanuel Knill, and Seth Lloyd. Dynamical decoupling of open quantum systems. *Physical Review Letters*, 82(12):2417, 1999.
- [37] Eisuke Abe, Hua Wu, Arzhang Ardavan, and John JL Morton. Electron spin ensemble strongly coupled to a three-dimensional microwave cavity. *Applied Physics Letters*, 98(25):251108, 2011.
- [38] Andrin Doll, Stephan Pribitzer, René Tschaggelar, and Gunnar Jeschke. Adiabatic and fast passage ultrawideband inversion in pulsed epr. *Journal of Magnetic Resonance*, 230:27–39, 2013.
- [39] James O’Sullivan, Oscar W Kennedy, Christoph W Zollitsch, Mantas Šimėnas, Christopher N Thomas, Leonid V Abdurakhimov, Stafford Withington, and John JL Morton. Spin-resonance linewidths of bismuth donors in silicon coupled to planar microresonators. *Physical Review Applied*, 14(6):064050, 2020.
- [40] Eisuke Abe, Alexei M Tyryshkin, Shinichi Tojo, John JL Morton, Wayne M Witzel, Akira Fujimoto, Joel W Ager, Eugene E Haller, Junichi Isoya, Stephen A Lyon, et al. Electron spin coherence of phosphorus donors in silicon: Effect of environmental nuclei. *Physical Review B*,

- 82(12):121201, 2010.
- [41] Richard E George, Wayne Witzel, H Riemann, NV Abrosimov, N Nötzel, Mike LW Thewalt, and John JL Morton. Electron spin coherence and electron nuclear double resonance of bi donors in natural si. *Physical Review Letters*, 105(6):067601, 2010.
- [42] Audrey Bienfait, JJ Pla, Yuimaru Kubo, Xin Zhou, Michael Stern, CC Lo, CD Weis, Thomas Schenkel, Denis Vion, Daniel Esteve, et al. Controlling spin relaxation with a cavity. *Nature*, 531(7592):74–77, 2016.
- [43] Eisuke Abe, Hua Wu, Arzhang Ardavan, and John J. L. Morton. Electron spin ensemble strongly coupled to a three-dimensional microwave cavity. *Applied Physics Letters*, 98(25):251108, 2011.
- [44] Crispin W Gardiner and Matthew J Collett. Input and output in damped quantum systems: Quantum stochastic differential equations and the master equation. *Physical Review A*, 31(6):3761, 1985.
- [45] Vishal Ranjan, Sebastian Probst, Bartolo Albanese, Andrin Doll, Oscar Jacquot, Emmanuel Flurin, Reinier Heeres, Denis Vion, Daniel Esteve, JLL Morton, et al. Pulsed electron spin resonance spectroscopy in the purcell regime. *Journal of Magnetic Resonance*, 310:106662, 2020.

Extended Data for Random-access quantum memory using chirped pulse phase encoding

James O'Sullivan,^{1,*} Oscar W. Kennedy,^{1,*} Kamanasish Debnath,² Joseph Alexander,¹
Christoph W. Zollitsch,¹ Mantas Šimėnas,¹ Akel Hashim,³ Christopher N. Thomas,⁴
Stafford Withington,⁴ Irfan Siddiqi,³ Klaus Mølmer,² and John J. L. Morton^{1,5}

¹*London Centre for Nanotechnology, UCL,
17-19 Gordon Street, London, WC1H 0AH, UK*

²*Department of Physics and Astronomy,
Aarhus University, DK-8000 Aarhus C, Denmark*

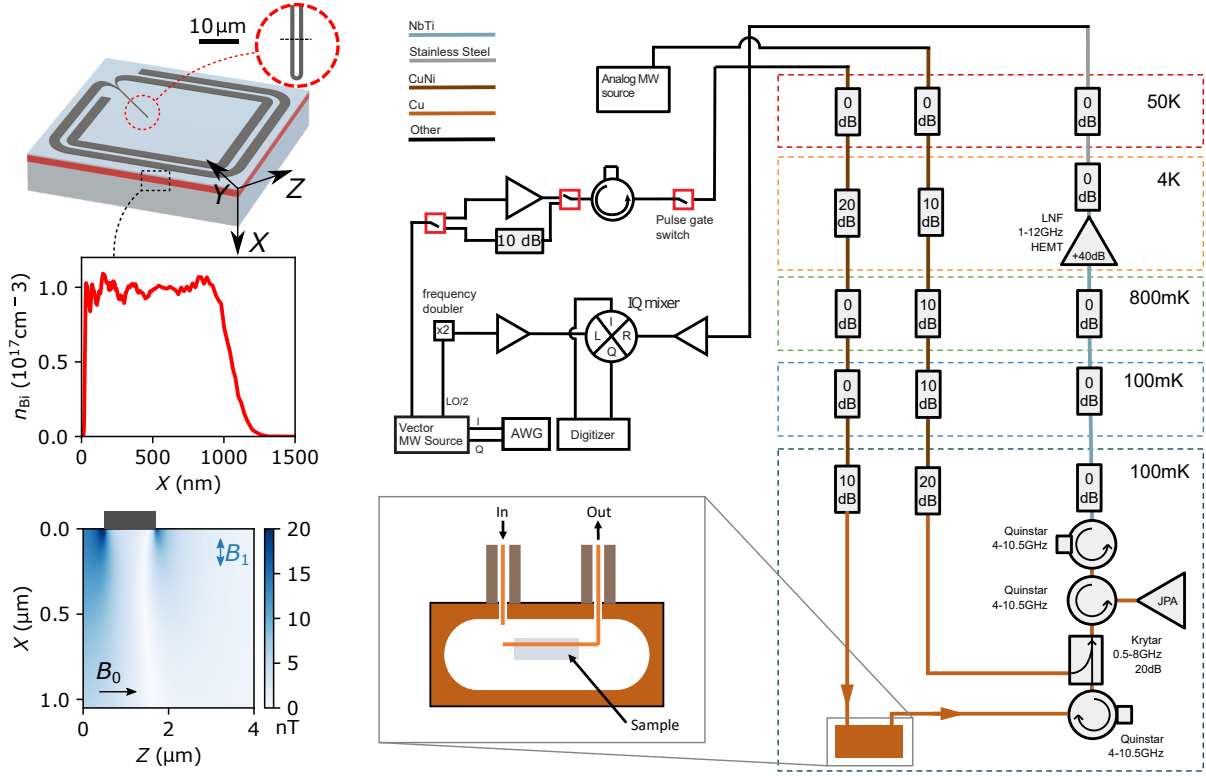
³*Lawrence Berkeley National Laboratory, Berkeley, CA 94720, USA*

⁴*Cavendish Laboratory, University of Cambridge,
JJ Thomson Ave, Cambridge CB3 0HE, UK*

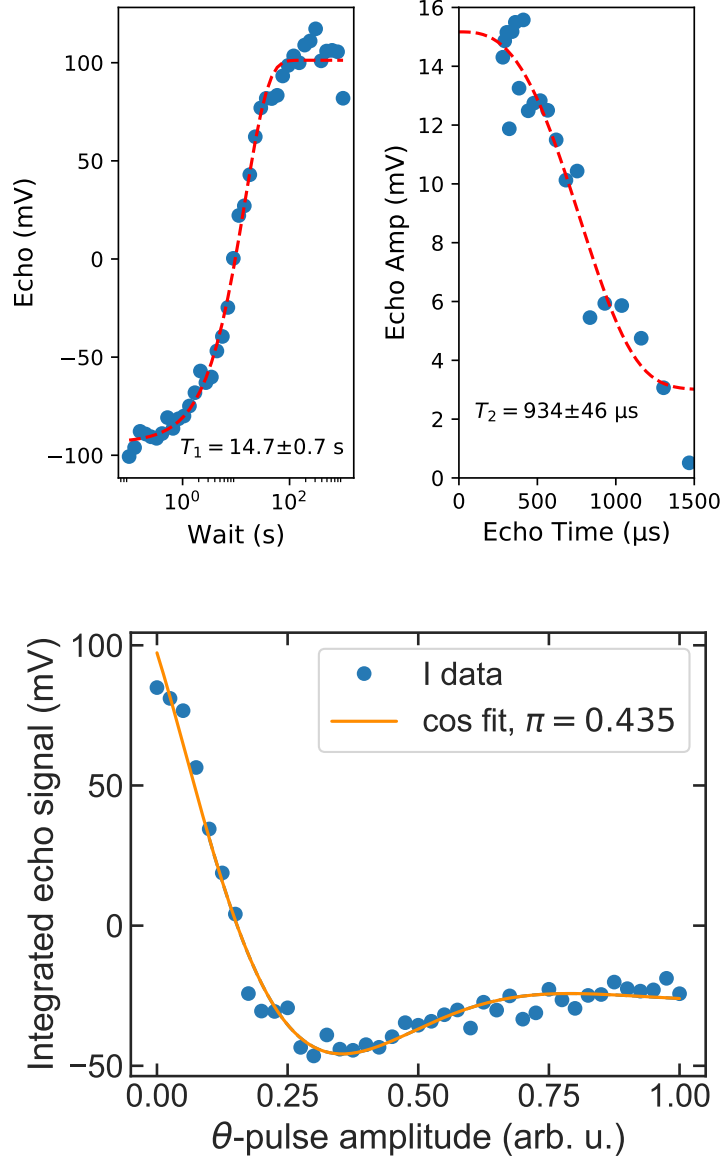
⁵*Department of Electrical and Electronic Engineering,
UCL, Malet Place, London, WC1E 7JE, UK*

arXiv:2103.11697v1 [quant-ph] 22 Mar 2021

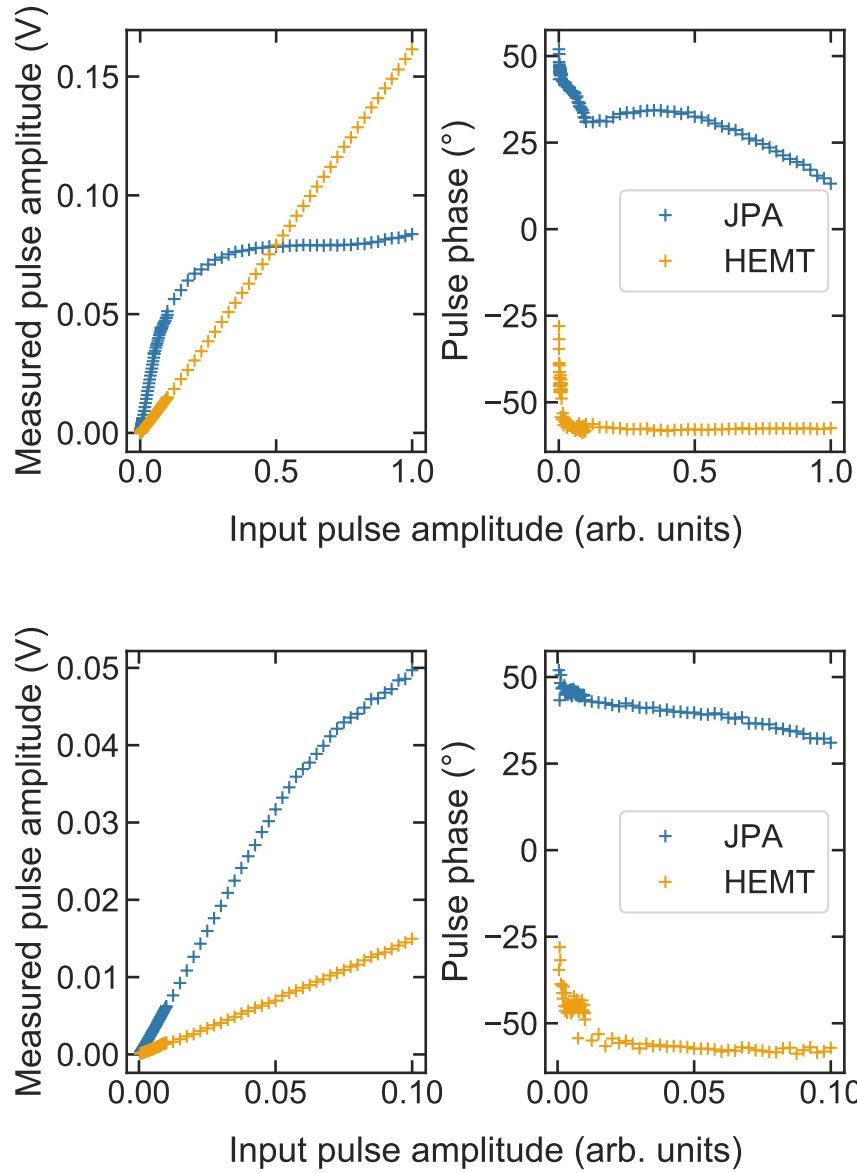
* These authors have contributed equally to this work



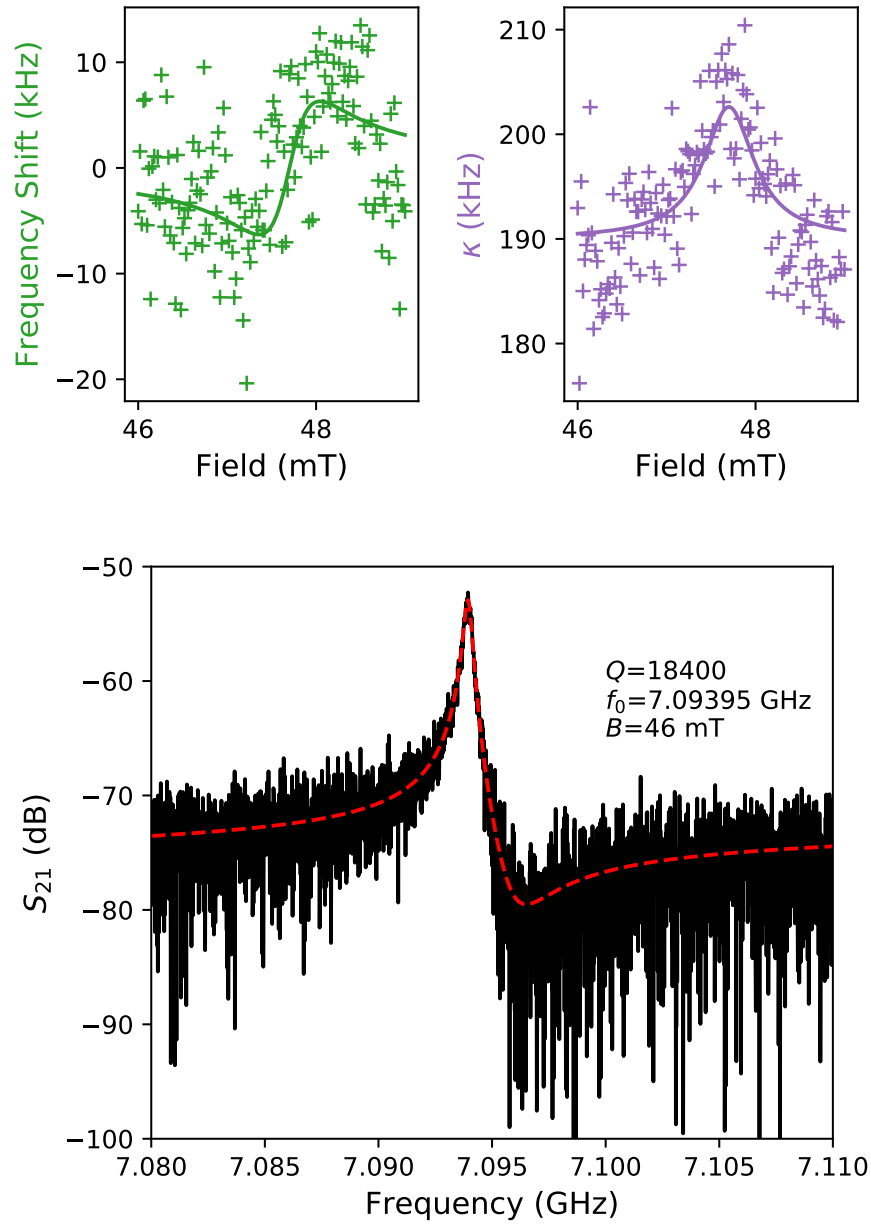
Extended Data Fig. 1. (a) Device schematic showing the double-back inductor. (b) The implanted bismuth profile determined by Monte-Carlo simulations. (c) Finite element modelling of the microwave magnetic field from zero-point fluctuations in the resonator. (d) Schematic of the spectrometer and dilution fridge setup. The copper box housing the cavity is magnified to show the configuration of the sample and antennae inside. The receive antenna is considerably longer than the input antenna to increase coupling to the cavity and maximise signal. Coaxial cable types inside the fridge have been colour coded.



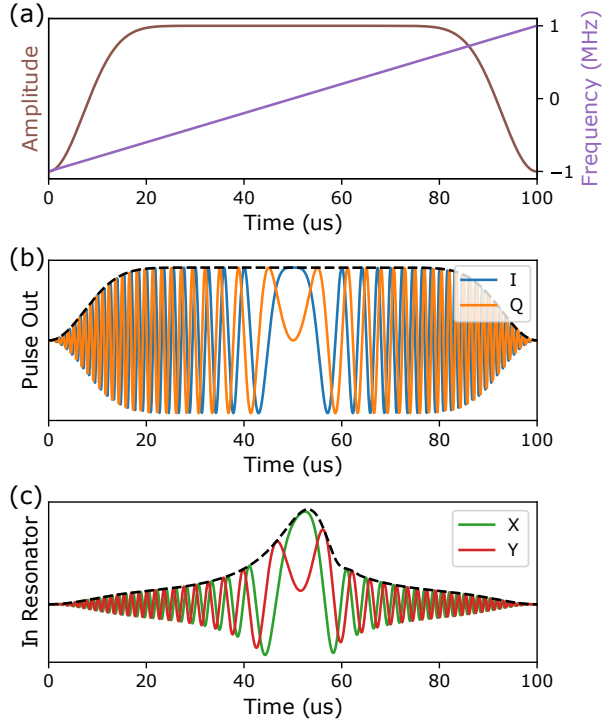
Extended Data Fig. 2. (a) T_1 by inversion recovery. A WURST pulse is used to invert the ensemble before a wait (indicated on the x axis) and a detection sequence at constant high power and τ . (b) T_2 measurement of the sample at the same weak excitation strength as used in Fig. 2 main text. The pulse sequence (inset) is a weak excitation followed by two 100 μ s WURST pulses. Increasing τ changes the echo time allowing T_2 to be measured. (c) Rabi oscillations using a gaussian θ -pulse of duration 8 μ s and FWHM 4 μ s and a two-WURST silenced echo detection sequence. The oscillations are heavily damped due to a large inhomogeneity in Rabi frequency across the ensemble.



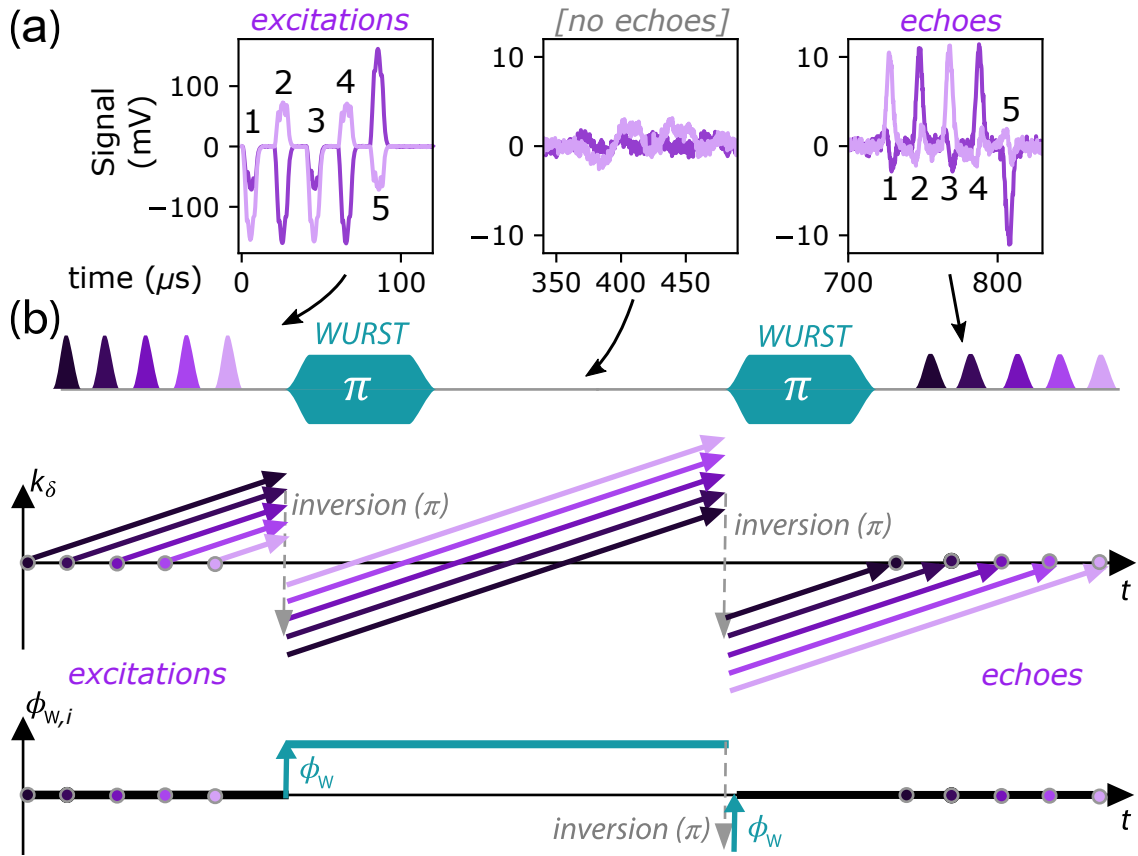
Extended Data Fig. 3. (a) Measured pulse amplitude as a function of input pulse amplitude, measured using the JPA (blue) and the HEMT without JPA (orange). (b) Low power regime of the same experiment.



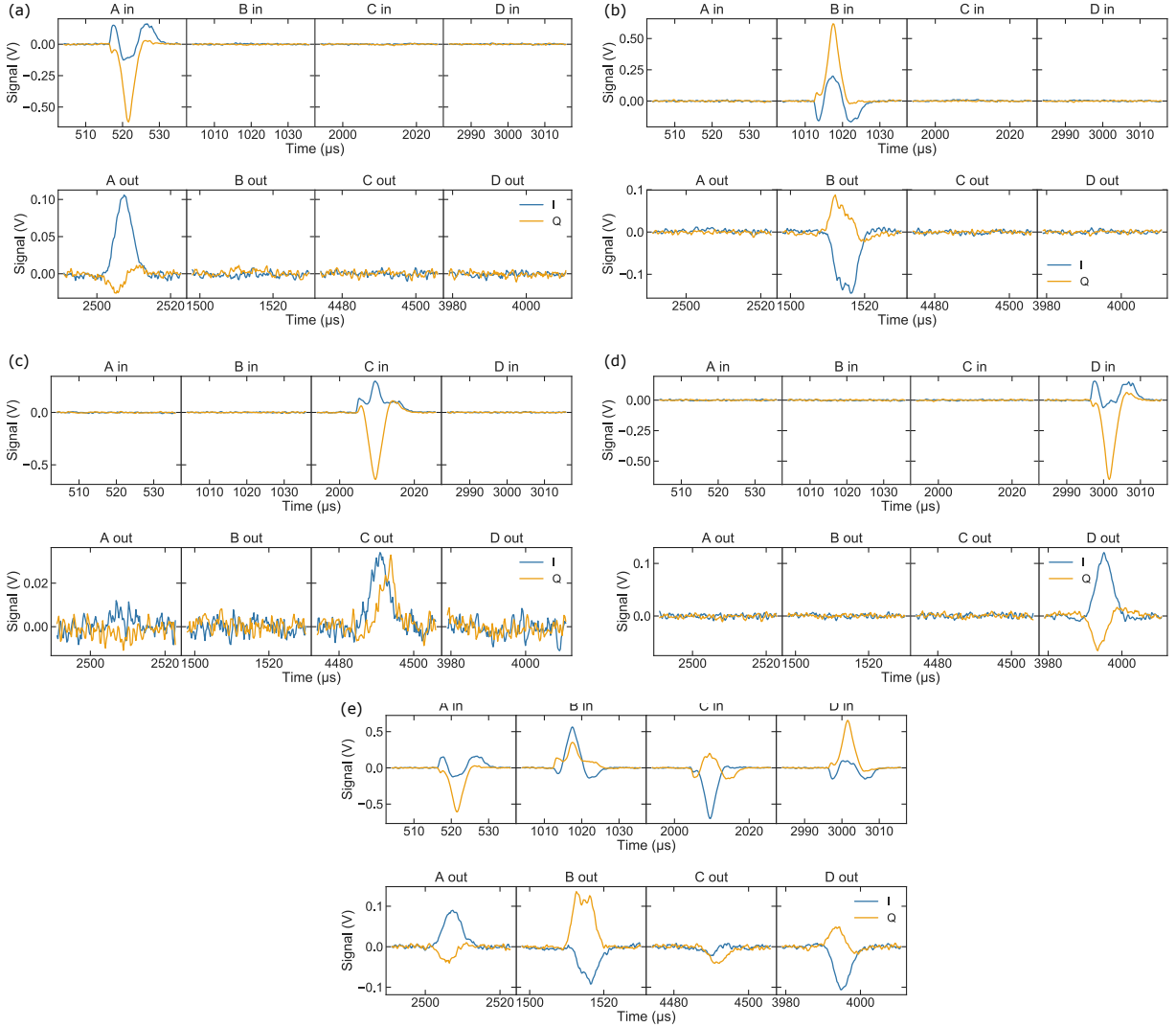
Extended Data Fig. 4. Effect of spins on (a) resonator frequency and (b) resonator linewidth κ as a function of magnetic field as the spin line passes through the resonator. Data are fit simultaneously to equations in Ref. [?] $g_{\text{ens}} \sim 120$ kHz and $\gamma \sim 1.2$ MHz. (c) Measurement of transmission magnitude through the copper cavity using a VNA at 46mT (off resonance with spin line). The superconducting resonator gives a characteristic Fano resonance response which we fit to extract a centre frequency for this resonator of 7.09395 GHz and a Q factor of 18400.



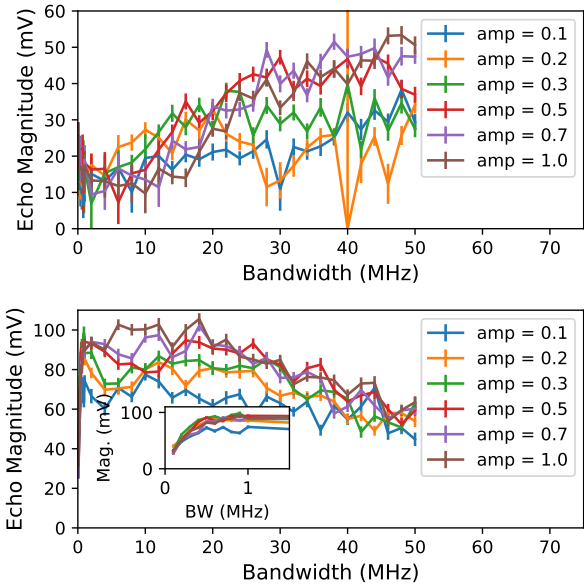
Extended Data Fig. 5. WURST-20 pulses with (a) the pulse amplitude and frequency shift for a WURST pulse with bandwidth 2 MHz and duration 100 μs . (b) The I and Q quadratures of the same WURST pulse. (c) The X and Y field quadratures in the cavity once the WURST pulse is filtered by the the $\kappa = 400$ kHz cavity.



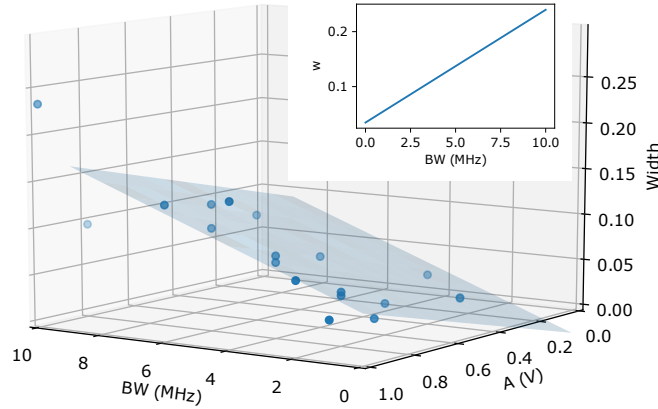
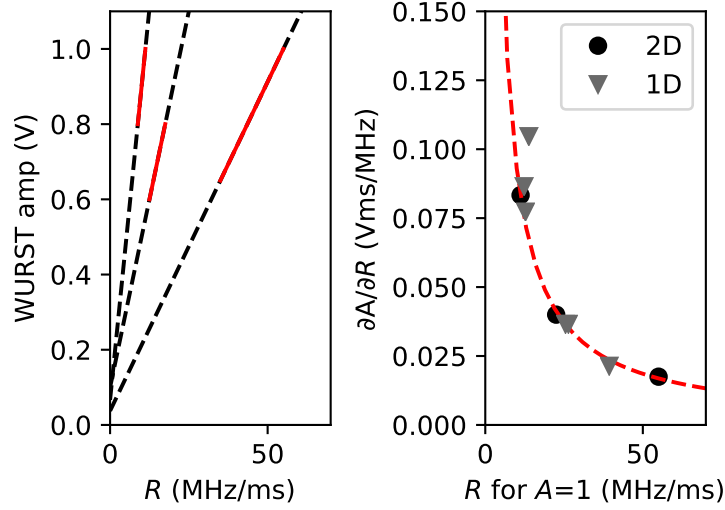
Extended Data Fig. 6. First in first out (FIFO) time bin encoding of multiple echoes. (a) An experimental demonstration of multiple excitations stored in FIFO protocol with WURST pulses. The pattern of excitation/echo phases allows echoes and excitations to be paired. (b) schematic showing evolution of spin waves and WURST phase resulting in the FIFO encoding with silenced excited echoes.



Extended Data Fig. 7. The memory sequence shown in Fig.3 was performed at higher input power (~ 500 photons per excitation pulse); the raw transient trace of the sequence is shown in (e). In Figs.(a-d) the same experiment was repeated with only one of each of the 4 input excitation pulses, A,B,C and D turned on. This allows us to unambiguously determine which echo originates from which excitation pulse. We see that a single echo appears in the expected read slot in each case. We also see that no other echoes appear when only one excitation is turned on. In this power regime, as well as amplifying (non-linearly), the JPA also imparts poorly characterized phase shifts seen particularly when comparing (c,d,e).



Extended Data Fig. 8. Top (bottom) panel – amplitude of the first (second), nominally silenced (unsilenced), echo as a function of the pulse bandwidth for 200 μ s WURST pulses. Inset to the bottom panel is the unsilenced data for low bandwidths, showing that there is a minimum bandwidth, similar to the cavity width, required to maximise the echo amplitude by refocusing all the spins in the cavity.



Extended Data Fig. 9. (a) The line of strong echoes from 2D maps of AB-echo sequences. We fit a line to these data and extract their gradient. (b) The gradient of the lines fit in (a) as a function of their extrapolated bandwidth at amplitude $A=1$ (black circles). The gradient determined when B-pulse has been swept in 1D in both amplitude and bandwidth are inferred and plot on the same axes (grey triangles) showing good agreement. We fit these data with $\partial A/\partial R = C/R$ with C a fit parameter and return the red dashed line and $C = 0.93$. (c) Width of the line of equivalent WURST pulses as a function of WURST pulse parameters. We fit a plane to this data to allow interpolation of the width as a function of bandwidth and amplitude.